ROYAL SOCIETY
OF CHEMISTRY

PAPER

How bulk and surface properties of Ti_4SiC_3, V_4SiC_3, Nb_4SiC_3 and Zr_4SiC_3 tune reactivity: a computational study†

Matthew G. Quesne, [ID] *[ab] C. Richard A. Catlow [ID] [abc] and Nora H. de Leeuw [ID] [ad]

We present several *in silico* insights into the MAX-phase of early transition metal silicon carbides and explore how these affect carbon dioxide hydrogenation. Periodic density functional methodology is applied to models of Ti_4SiC_3, V_4SiC_3, Nb_4SiC_3 and Zr_4SiC_3. We find that silicon and carbon terminations are unstable, with sintering occurring in vacuum and significant reconstruction taking place under an oxidising environment. In contrast, the metal terminated surfaces are highly stable and very active towards CO_2 reduction. However, we predict that under reaction conditions these surfaces are likely to be oxidised. These results are compared to studies on comparable materials and we predict optimal values for hydrogen evolution and CO_2 reduction.

Introduction

The H-(Hägg)phase of over 100 ternary carbides/nitrides was first identified in the 1960s.[1,2] This class of material is also given the annotation "MAX"-phase, an abbreviation of the general formula of these 2D materials '$M_{n+1}AX_n$', where M denotes an early transition metal and A/X represent an A group element and carbon/nitrogen, respectively.[3–5] Importantly, these initial studies also found that these materials possess a novel mixture of chemical properties, including the high thermo-/electrical-conductivity of a metal and a resistance to thermo/ oxidative shocks more typical of a ceramic.[1,6–10] Owing to this set of novel properties these materials are also called "metallic ceramics".[11] Interestingly, this same mixture of properties is also present in the closely related monocarbide materials which in recent years have received a lot of interest from the catalytic

*a*School of Chemistry, Cardiff University, Main Building, Park Place, Cardiff CF10 3AT, UK. E-mail: quesnem@ cardiff.ac.uk

*b*UK Catalysis Hub, Research Complex at Harwell, STFC Rutherford Appleton Laboratory, Didcot, Oxfordshire OX11 0FA, UK

*c*Department of Chemistry, University College London, 20 Gordon St., London WC1H 0AJ, UK

*d*School of Chemistry, University of Leeds, Leeds LS2 9JT, UK

community owing to their activity in many important industrial processes, including CO oxidation,[12,13] various hydrogenation[14] and the water–gas shift[15,16] reactions. Importantly, for our work as well as the theme of this *Faraday Discussions* meeting, these carbides have also been shown effectively to hydrogenate CO_2 to useful chemicals.[17–20]

Structurally, the (0001) basal plane of silicon carbides strongly resembles the pristine (111) facets of early transition metal carbides (TMCs), which are the facets that have been shown to be most efficient at catalysing the hydrogenation of CO_2.[17,21] Indeed, detailed *in silico* investigations by our group clearly indicate that the metal terminated (111) surfaces of the equivalent TMCs to the MAX-phase silicon carbides investigated here are extremely active toward CO_2 activation.[22] Expectations for the performance of these materials has also been informed by recent modelling work into another closely related class of material, *i.e.* the MXene-phase of early transition metal carbides, which also show a remarkable selectivity for carbon capture/utilisation.[23–25] Again, the (0001) facet of these materials shows a remarkably similar topology to the metal terminated facet of silicon carbides. However, the MAXene stoichiometry of M_2C leads to the production of two metal terminations, instead of the facets with one metal termination and one termination by either carbon or silicon, as seen in the silicon carbides discussed in this work. The choice of the transition metal components was partly informed by these studies and partly by a systematic screening of the bulk and surface properties of a diverse array of carbides.[26] The latter suggested that the early transition metals had the most promising combination of surface properties for the catalysis of CO_2 reduction by hydrogen. Therefore, this paper presents the results from a computational study into the bulk and catalytic properties of Ti_4SiC_3, V_4SiC_3, Nb_4SiC_3 and Zr_4SiC_3 and compares these properties to those already obtained for TiC, VC, NbC and ZrC.

Methodology

Unless otherwise stated, all energies were obtained using the standard Perdew–Burke–Ernzerhof (PBE) functional[27] in combination with the Vienna *Ab initio* Simulation (VASP) Package.[28–30] Benchmark studies, using formation energies for these materials with both RPBE[45] and PBEsol,[46] have produced consistent values for all methods which validates our choice of methodology. Such a protocol has been shown to be sufficient for replicating experimental trends for both surface properties and reactivities of closely related carbide[26] and MXene materials.[25] Plane-wave basis sets are applied to valence electrons with core potentials produced using projected augmented wave methodology (PAW)[31] to describe the core electrons of each element. Long-range dispersion interactions were introduced *via* the D3 method.[32,33] Bulk structures for α-Ti_4SiC_3 (ref. 7) and α-Nb_4SiC_3 (ref. 34) were taken from the Inorganic Structure Database (ICSD),[35] whilst the MAX-phase of α-V_4SiC_3 and α-Zr_4SiC_3 were created by *in silico* modification of the former structures. The lattice parameters and the internal coordinates of each material were then fully optimized for all degrees of freedom and the (0001) basal plane was cut between the metal–carbon and metal–silicon layers using the METADISE code.[36] Since the materials consist of alternating layers of metal and either carbon or silicon, only two possible slabs can be constructed in this plane: both express one metal layer, with one slab also terminated by carbon and the

other slab terminated by the corresponding silicon surface. This sequence is due to the stoichiometry of these materials with a 1 : 1 ratio of metal to either carbon or silicon. The primitive cell of each silicon carbide was replicated into a $2 \times 2 \times 2$ simulation cell to give slabs with nine atoms in each layer and 16 atomic layers along the z-axis to give a total of 144 atoms per slab. Above each termination was placed 15 Å of vacuum. A fine Monkhorst–Pack grid with a $5 \times 5 \times 5$ k-point mesh was applied to all bulk calculations, with surface properties being determined using a $5 \times 5 \times 1$ mesh. In all cases, energies were converged to within 520 eV and a threshold of 0.01 eV Å^{-1} was used for geometry optimisations. Self-consistency cycles (SCF) were converged to within 10^{-5} eV and the Blöchl smearing method was applied for higher accuracy.[37] In all cases, half of each slab (the top 8 layers) was allowed to relax fully, whilst the bottom 8 layers were fixed to maintain their bulk-optimised positions. Spin polarization was also enabled to account for the magnetic moments in the materials and electron transfer during catalysis.

Adsorption energies for H_2O, H_2, O_2, OH and CO_2 are defined as:

$$E_{ads} = E_{(slab/molec)} - [E_{(slab)} + E_{(molec)}], \tag{1}$$

where the sum of the energies of the pristine slab and gas phase adsorbate(s) are subtracted from the total energy of the minimum energy structure of the slab with adsorbates. Vibrational frequencies, calculated with the finite difference method, confirmed the global minima for all absorbed species.

Results

Bulk properties

MAX-phase silicon carbide crystal structures for α-Ti_4SiC_3 (ref. 7) and α-Nb_4SiC_3 (ref. 34) were taken from the Inorganic Structure Database (ICSD).[35] Since no structures were available for α-V_4SiC_3 and α-Zr_4SiC_3, they were created in silico by exchanging the transition metal component and running full optimisations of both the lattice parameters and atomic coordinates. For a meaningful comparison, the same bulk references for the individual elements were used as previously reported for the carbides,[26] with the addition of an elemental silicon reference.[38] Our results show that the addition of interstitial silicon layers into the carbide

Table 1 Energies of formation (O_fE^0) for each silicon carbide compared to the corresponding monocarbide material (with the same metal component). All values are normalised to eV per atom and compared with the experimental heat of formation

	$^aO_fE^0$	$^bO_fE^0$	$^cO_fE^0$	$^dO_fH^0$
TiC	−0.830	−0.915	−0.836	−0.951 (ref. 39)
Ti_4SiC_3	−0.863	−0.933	−0.848	
VC	−0.439	−0.558	−0.425	−0.524 (ref. 39)
V_4SiC_3	−0.518	−0.363	−0.501	
ZrC	−0.950	−1.010	−0.933	−0.959 (ref. 39)
Zr_4SiC_3	−0.937	−0.996	−0.915	
NbC	−0.551	−0.622	−0.613	−0.676 (ref. 39)
Nb_4SiC_3	−0.563	−0.632	−0.562	

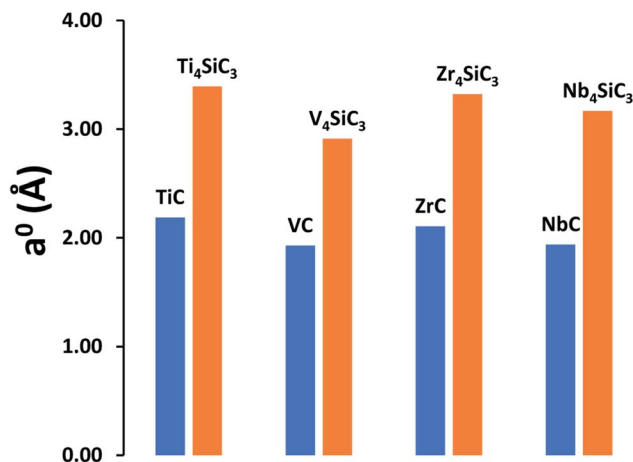^{a} PBE. ^{b} PBE$_{sol}$. ^{c} RPBE. ^{d} Experimental values.

Fig. 1 Comparison of lattice constants (a^0) for both the monocarbides and their comparable silicon carbides. All results are calculated using the PBE functional.

lattice has a relatively small effect on formation energies (see Table 1) with no consistent trend observed, although silicon addition does appear to have a very large effect on the relative lattice constants (Fig. 1), which is unsurprising since at 210 pm silicon has the largest atomic radius of any of the elements in the materials under investigation. This effect is most apparent when examining the relative surface areas of the carbide (111) and silicon carbide (0001) facets, which have the same number of atomic sites in both facets, where the relative values are as follows: Ti_4SiC_3 (149.04 $Å^2$) *vs.* TiC (139.79 $Å^2$); V_4SiC_3 (132.30 $Å^2$) *vs.* VC (125.09 $Å^2$); Zr_4SiC_3 (175.33 $Å^2$) *vs.* ZrC (162.36 $Å^2$); and Nb_4SiC_3 (157.15 $Å^2$) *vs.* NbC (149.99 $Å^2$).

Density of states

Total density of states plots for each of the materials are shown in Fig. 2. Importantly, all four materials are clearly metallic in nature, with some bands crossing the Fermi level.

Decomposition of these states indicates that there is a high level of hybridization between 3d or 4d orbitals of the metal with both the 2p states of the carbon and 3s orbitals of the silicon. All these materials, therefore, show considerable amounts of M–C and M–Si covalency. These same general properties were also reported previously for the related monocarbide materials,[26] and our results replicate previously reported electronic structure analysis for α-Nb_4SiC_3.[34] There is also the same apparent increase in peak intensity in the group 5 over the group 6 metals that in carbides has been associated with a decrease in the strength of the M–C bond and an increase in ionic character.[40] This shift is primarily due to an increase in the number of valence d-electrons and also causes a negative shift in the position of the d-band centre in relation to the Fermi level. Finally, the density of states in the conduction band is much higher in the silicon-containing carbides with d^2 metals (*i.e.* the metals in group 4 with the valence electrons d^2, s^2) than for the d^3 which could indicate greater redox potential in the former.
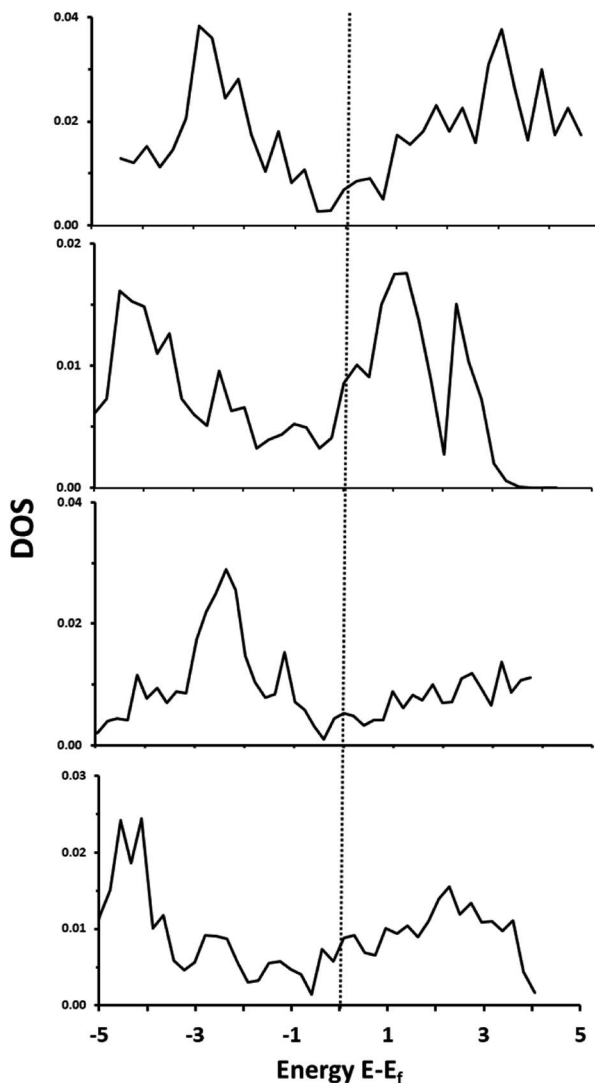
Fig. 2 Total DOS of: α-Ti$_4$SiC$_3$ (top), α-V$_4$SiC$_3$ (second from top), α-Zr$_4$SiC$_3$ (second from bottom), α-Nb$_4$SiC$_3$ (bottom).

To a large extent, catalytic activity as well as other surface properties, such as the stability of different facets, can be linked to surface energies (σ), and work functions (Φ).[41] We have calculated these properties for each silicon carbide by cleaving along the (0001) plane and allowing the uppermost half of the slab to relax; depictions of the morphology of each relaxed surface can be found in Fig. S1 (see ESI†). Interestingly, major reconstruction (leading to surface-mediated formation of elemental silicon) is observed when the silicon-terminated surfaces of the 3d silicon carbides are relaxed, which indicates that the M–Si bond broken is far weaker than the new Si–Si bonds formed. Relaxed surface energies (σ) were calculated using eqn (2) and (3). A denotes the area of each

surface, where E_{slab} signifies the total surface energy and n denotes the number of unit cells used for each slab. When calculating the energy to create two unrelaxed surfaces (eqn (2)) 2 is added to the denominators.

$$\sigma^u = \frac{E_{slab} - nE_{bulk}}{2A} \tag{2}$$

$$\sigma^r = \frac{E_{relax} - nE_{bulk}}{A} - \sigma^u \tag{3}$$

When only half the slab is relaxed, the relaxation component of the surface energy (σ) must be determined, as shown in eqn (3); here the area of only one surface is included in the denominator and this energy is subtracted from that of the unrelaxed surfaces. The computed σ for various facets of both the silicon-containing carbides reported here and their corresponding monocarbide equivalents are shown in Table 2. Previous work by our group showed that relaxing only the surface layers of the (111) facets of the corresponding monocarbides was critically important in both explaining the energetic differences between the two very different facets and to maintain the constraints provided by the bulk properties.[26] From the values in Table 2, it is clear that surface energies for the carbon-terminated slabs in both the monocarbide and silicon carbide materials are very high.

The silicon carbide (0001) slabs with both silicon and metal terminations have much lower surface energies, closer to the dominant (001) surface of the monocarbides than to the (111) facets. This result is perhaps unsurprising since in the presence of absorbates the carbon terminated (111) facet of early transition metal carbides has been shown to be extremely unstable and therefore would only be expected as a meta-stable phase under vacuum conditions.[22,42] Fig. S1† shows that there is a major reconstruction of both the silicon and carbon terminated surfaces upon relaxation. To attempt to see if this major surface reconstruction also occurs in an oxygen-rich environment, we have also added a monolayer of eight oxygen atoms to each pristine termination; however, upon optimisation, various partially oxidised silicon and carbon species were formed in all cases (see Fig. S2, ESI†). Owing to their potential instability and relatively high surface energies, it is clear

Table 2 Relaxed surface energies (σ) and surface areas (a^2) for each possible termination of the four silicon containing carbides compared to values for the (001) and metal terminated (111) surfaces of the corresponding monocarbides.[26] All surface energies are given in J m^{-2} with the corresponding areas shown in Å^2

	[a]SiC [a]σ^2	[b]SiC [b]σ^2	[a,b]a^2	[c]SiC [c]σ^2	[c]a^2	[d]C [d]σ^2	[d]a^2	[e]C [e]σ^2	[f]C [f]σ^2	[e,f]a^2
Ti	2.822	3.095	139.79	6.337	139.79	2.190	79.89	5.615	5.891	149.04
V	3.127	3.853	125.09	5.116	125.09	1.927	70.53	4.742	4.938	132.30
Zr	2.641	2.891	162.36	5.962	162.36	2.106	102.63	5.043	5.086	175.33
Nb	3.012	2.104	149.99	5.507	149.99	1.937	79.87	4.709	4.347	157.15

[a] Metal silicon facets, metal layer relaxed. [b] Metal silicon facets, silicon layer relaxed. [c] Metal carbon facets, carbon layer relaxed. [d] (001) monocarbide facet. [e] (111) metal terminated carbide facet. [f] (111) carbon terminated facet.

that the carbon and silicon terminated (0001) facets of these silicon carbides will be unstable under reaction conditions and that the surface morphology of the catalysts will be either dominated by pristine metal surfaces or by sintered coke/ elemental silicon on top of a metal surface support. Therefore, unless otherwise stated, the remainder of this study will focus on the activity of the metal terminated (0001) facets.

Reactivity on the pristine surfaces

Hydrogen adsorption. We attempted to identify barriers for hydrogen adsorption by performing geometry scans that sequentially lower physically adsorbed hydrogen from the vacuum to the silicon carbide surfaces. To this end, each hydrogen molecule was fixed in the z-direction and sequentially lowered towards the surface, but allowing full relaxation along all other degrees of freedom. The resulting energies of these scans are shown in Table S3 (see ESI†). However, whilst no local minima in such stepwise pathways to adsorption were found, the subsequent chemical adsorption step was shown to be a barrierless and extremely exothermic process. Since the same barrierless adsorption mechanism has been reported previously for the metal terminated (111) surfaces of the corresponding monocarbides,[42] we will continue our study by examining hydrogen loading effects on these facets.

Fig. 3 shows the adsorption energies for the most exothermic adsorption modes of hydrogen under various coverages on the pristine metal terminated surfaces of the four silicon carbides considered in this study. The trends reported here are very similar to those reported previously for the metal terminated (111) facets of the corresponding monocarbides,[42] where it was demonstrated that the decrease in adsorption energies with higher loading of hydrogen is primarily due to electronic effects, whereby electron donation into the conduction band of the carbides increases the surface work function. The same phenomenon is observed here, with a steeper slope obtained for the silicon carbides with group 5 transition metals owing to their increased number of electrons in the d-bands exacerbating
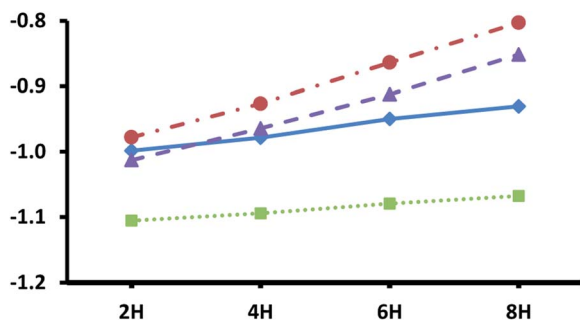

Fig. 3 Adsorption energies for different hydrogen loadings on top of pristine metal terminated surfaces of four MAX-phase silicon carbides. Values are shown for: Ti_4SiC_3 blue diamonds (solid trend line), V_4SiC_3 brown circles (dotted and dashed trend line), Zr_4SiC_3 green squares (dotted trend line) and Nb_4SiC_3 purple triangles (dashed trend line). Energies are given in eV per atom with reference to gas phase molecular hydrogen. Number of hydrogen atoms added is given along the x-axis in multiples of two (i.e. indicating increasing molecules of H_2 added).

Faraday Discussions

this effect. Unfortunately, whilst smaller than those observed for the metal terminated (111) surfaces of the monocarbides (almost certainly due in part to the higher surface energies of those facets) the hydrogen adsorption energies here may still be too large at even the highest loadings for the adsorbed hydrogen to be useful for efficient CO_2 reduction. This prediction is informed by our previous work, where very similar hydrogen adsorption energies on the (111) surfaces of the corresponding monocarbides makes those facets less than ideal for hydrogenation processes under reaction conditions.[42]

Carbon dioxide adsorption. The adsorption energies for the lowest energy chemical adsorption modes for CO_2 on top of the metal terminated (0001) facets of the four MAX-phase catalysts are shown by the orange bars in Fig. 4 and are considerably more exothermic than the energies previously reported for the monocarbide surfaces[22] for all materials except for V_4SiC_3, which is calculated to lead to a very similar adsorption energy to that of the metal terminated (111) surface of VC. The values that we present here correlate more closely to values obtained for MAXenes with M_2C stoichiometry, for which adsorption energies of -3.69 for Ti_2C and -3.16 for Zr_2C were calculated.[43] Important geometric and electronic information about the lowest energy adsorption modes for carbon dioxide on top of each silicon carbide surface is given in Fig. S5, ESI.† These data show that whilst the average metal oxygen bond distance between the surface and adsorbate is modulated almost completely by the ideal M–C bond distance the amount of charge transfer (and corresponding elongation of the C–O bond length) varies depending on the periodic position of the parent transition metal. Importantly, group IV metals (Ti/V) see an increase of ~ 0.6 in number of electrons transferred to the CO_2 upon adsorption from the values observed for their V metal equivalents (Zr/Nb), which corresponds to both greater activation of the adsorbate and a more exothermic adsorption energy. Additionally, modelling of MAXenes with a M_3C_2 stoichiometry and d^3 transition metals predicted much smaller
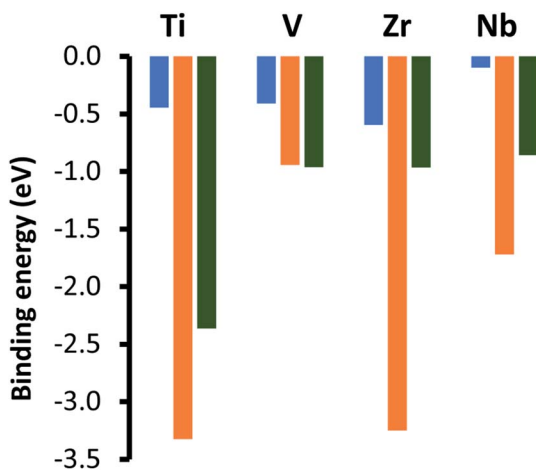

Fig. 4 Adsorption energies for chemically adsorbed carbon dioxide on the metal terminated (0001) basal plane of the four silicon carbides, shown by the orange bars. These values are compared to adsorption energies for the comparable (001) (blue bar) and metal terminated (111) (green bar) surfaces of the comparable monocarbide catalysts [ref. 22].

adsorption energies of −2.19 for V_3C_2 and −2.35 for Nb_3C_2.[23] Whilst high carbon dioxide capture on the pristine facets is more reminiscent of the MAXene-phase than the metal terminated (111) facets of the fcc-monocarbides, the adsorption energies are still slightly smaller than those on the MAXenes. Such high energies in the MAXenes are explained by the absence of a free (pristine) metal surface under either synthesis or reaction conditions. Indeed, all these materials are capped by a terminating layer of either OH, O, F or H monolayers.[44] Therefore, the remainder of this paper will focus on the effects of monolayer formation on the metal facet of MAX-phase silicon carbides.

Atomic monolayer formation and reactivity

First, we consider solvation of the surfaces in an aqueous environment. The energy per molecule of eight water molecules adsorbed on each surface is shown in Fig. 5 and there is little variation between the values for each material, which range between −1.03 for V_4SiC_3 to −0.91 for Zr_4SiC_3. To create each layer, water molecules were initially placed in the most exothermic binding motifs (corresponding to the highly coordinated hollow sites) after which other molecules were sequentially added to fill each surface, whilst every attempt was made to maximise hydrogen-bonding networks between molecules. The extent to which this was possible was largely determined by surface structure, as is also shown in Fig. 5, where the bottom panels show the hydrogen-bonding energy per molecule, obtained after the surface was removed and a single point energy calculation was performed. These results show that for each silicon carbide surface, except for Zr_4SiC_3 (where the network is much weaker), the surface-mediated hydrogen-bonding networks maintain approximately half the energy of each hydrogen-bond formed by water under atmospheric conditions. The anomalous value for Zr_4SiC_3 is possibly due to the larger distances between binding sites caused by the larger surface area.

Finally, we examined surface modifications under oxidising environments. Fig. 6 shows the morphology and energetics of a fully oxidised or hydroxylated metal terminated (0001) surface for each catalyst. The references for the surface
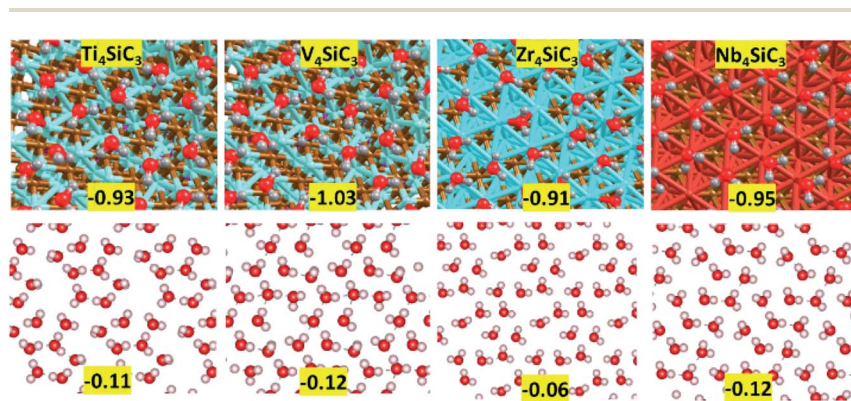

Fig. 5 Water monolayers on top of exposed metal terminated (0001) basal plane of silicon carbides. (top) Adsorption energy in eV per H_2O for eight water molecules adsorbed on each surface. (bottom) Hydrogen-bonding energy in eV per H_2O for the water layer without the surface interactions.
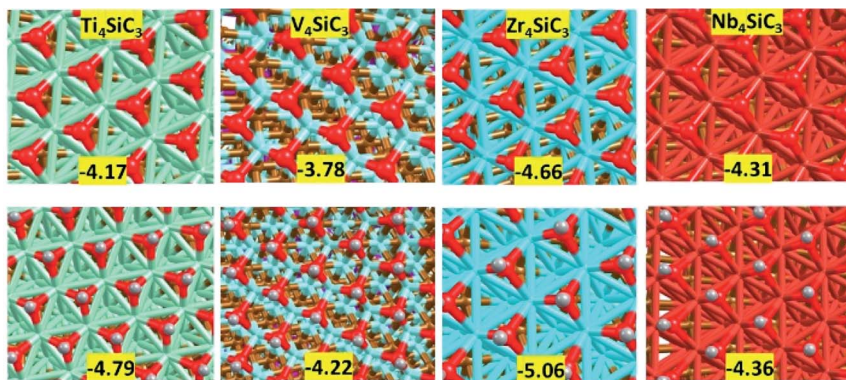
Fig. 6 Models of oxidised surfaces of the four metal terminated silicon carbides. (top) Oxygen monolayer of nine oxygen atoms with energies given in eV per O_{atom}. (bottom) Hydroxylated surfaces with nine −OH groups per surface with values given in eV per $OH_{molecule}$.

formation energies are triplet oxygen and singlet hydrogen molecules in the gas phase. Importantly, the oxide and hydroxide layers on this surface are formed without major modification to the rest of the slab which contrasts strongly with the results obtained using the carbon and silicon terminations (see ESI Fig. S2†). The addition of other adlayers has an extremely exothermically favourable stabilising effect that again is in excellent agreement with previous experimental results from the related MAXene-phases.[44] More interestingly, by subtracting the energies for the formation of the oxide layers from those of the hydroxyl layers, we observe a large reduction in the hydrogen adsorption values: Ti_4SiC_3 pristine (−0.93 eV per H) *vs.* oxidised (−0.62 eV per H); V_4SiC_3 pristine (−0.80 eV per H) *vs.* oxidised (−0.44 eV per H); Zr_4SiC_3 pristine (−1.07 eV per H) *vs.* oxidised (−0.40 eV per H); and Nb_4SiC_3 pristine (−0.85 eV per H) *vs.* oxidised (−0.05 eV per H). These latter energies are interesting, because they are close to the values determined *via* modelling of chemical potentials to be optimal for the CO_2 hydrogenation reaction over the monocarbide materials.[22] However, it is still unknown whether these hydroxylated surfaces will also maintain their other catalytic properties that make silicon carbide MAX-phases such exciting candidates for CCC and CCU processes.

Conclusions

The MAX-phases of early transition metal silicon carbides represent an interesting class of materials, owing to both their novel mix of metallic, covalent and ionic properties, as well as their structural similarities to related redox catalysts for carbon utilisation reactions. Our results demonstrate that the silicon and carbon terminations of these materials are unstable, with strong silicon–silicon and carbon–carbon bonds causing sintering and coking respectively, when undercoordinated atomic layers are exposed to the vacuum. In the presence of oxygen these terminations lead to the formation of partially oxidised silicon- and carbon-containing species as well as massive surface reconstruction. However, these materials can also terminate at an extremely stable metal (0001) facet that is very active towards CO_2 adsorption and activation. Unfortunately, these facets

adsorb hydrogen far too strongly for them to be useful for the hydrogenation of carbon dioxide, although further calculations suggest that oxidised surfaces may have the ideal properties for this process. Finally, whilst these materials appear to show many promising characteristics as potential CCU catalysts, much more experimental and theoretical work is required to study their activity and selectivity towards the production of industrially useful chemicals.

Conflicts of interest

There are no conflicts to declare.

Acknowledgements

Notes and references

1 M. W. Barsoum, The MN+1AXN phases: a new class of solids, *Prog. Solid State Chem.*, 2000, **28**, 201–281.

2 W. Jeitschko, H. Nowotny and F. Benesovsky, Kohlenstoffhaltige ternäre Verbindungen (H-Phase), *Monatsh. Chem.*, 1963, **94**, 672–676.

3 Z. M. Sun, Progress in research and development on MAX phases: a family of layered ternary compounds, *Int. Mater. Rev.*, 2011, **56**, 143–166.

4 M. W. Barsoum and T. El-Raghy, New phases: carbide and nitride materials unique ternary ceramics turn out to be surprisingly soft and machinable, yet also heat-tolerant, strong and lightweight, *Am. Sci.*, 2001, **89**, 334–343.

5 W. Jeitschko and H. Nowotny, Die Kristallstruktur von Ti3SiC2-ein neuer Komplexcarbid-Typ, *Monatsh. Chem.*, 1967, **98**, 329–337.

6 P. Eklund, M. Beckers, U. Jansson, H. Högberg and L. Hultman, *Thin Solid Films*, 2010, **518**, 1851–1878.

7 E. H. Kisi, J. A. A. Crossley, S. Myhra and M. W. Barsoum, Structure and crystal chemistry of Ti3SiC2, *J. Phys. Chem. Solids*, 1998, **59**, 1437–1443.

8 T. El-Raghy, A. Zavaliangos, M. W. Barsoum and S. R. Kalidindi, Damage Mechanisms around Hardness Indentations in Ti3SiC2, *J. Am. Ceram. Soc.*, 2005, **80**, 513–516.

9 M. W. Barsoum, T. El-Raghy and L. U. J. T. Ogbuji, Oxidation of Ti3SiC2 in air, *J. Electrochem. Soc.*, 1997, **144**, 2508–2516.

10 T. El-Raghy and M. W. Barsoum, Diffusion kinetics of the carburization and silicidation of Ti3SiC2, *J. Appl. Phys.*, 1998, **83**, 112–119.

11 Z. M. Sun, H. Hashimoto, Z. F. Zhang, S. L. Yang and S. Tada, Synthesis and Characterization of a Metallic Ceramic Material–Ti3SiC2, *Mater. Trans.*, 2006, **47**, 170–174.

12 L. K. Ono, D. Sudfeld and B. Roldan Cuenya, In situ gas-phase catalytic properties of TiC-supported size-selected gold nanoparticles synthesized by diblock copolymer encapsulation, *Surf. Sci.*, 2006, **600**, 5041–5050.

13 K.-Z. Qi, G.-C. Wang and W.-J. Zheng, A first-principles study of CO hydrogenation into methane on molybdenum carbides catalysts, *Surf. Sci.*, 2013, **614**, 53–63.

14 P. M. Patterson, T. K. Das and B. H. Davis, Carbon monoxide hydrogenation over molybdenum and tungsten carbides, *Appl. Catal., A*, 2003, **251**, 449–455.

15 P. Lui and J. A. Rodriguez, Water-Gas-Shift Reaction on Molybdenum Carbide Surfaces: Essential Role of the Oxycarbide, *J. Phys. Chem. B*, 2006, **110**, 19418–19425.

16 N. M. Schweitzer, J. A. Schaidle, O. K. Ezekoye, X. Pan, S. Linic and L. T. Thompson, High Activity Carbide Supported Catalysts for Water Gas Shift, *J. Am. Chem. Soc.*, 2011, **133**, 2378–2381.

17 M. D. Porosoff, S. Kattel, W. Li, P. Liu and J. G. Chen, Identifying trends and descriptors for selective CO_2 conversion to CO over transition metal carbides, *Chem. Commun.*, 2015, **51**, 6988–6991.

18 C. Kunkel, F. Viñes and F. Illas, Transition metal carbides as novel materials for CO2 capture, storage, and activation, *Energy Environ. Sci.*, 2016, **9**, 141–144.

19 S. Posada-Pérez, F. Viñes, P. J. Ramirez, A. B. Vidal, J. A. Rodriguez and F. Illas, The bending machine: CO2 activation and hydrogenation on δ-MoC(001) and β-Mo2C(001) surfaces, *Phys. Chem. Chem. Phys.*, 2014, **16**, 14912–14921.

20 M. D. Porosoff, X. Yang, J. A. Boscoboinik and J. G. Chen, Molybdenum Carbide as Alternative Catalysts to Precious Metals for Highly Selective Reduction of CO_2 to CO, *Angew. Chem., Int. Ed.*, 2014, **53**, 6705–6709.

21 C. Kunkel, F. Viñes and F. Illas, Transition metal carbides as novel materials for CO_2 capture, storage, and activation, *Energy Environ. Sci.*, 2016, **9**, 141–144.

22 M. G. Quesne, A. Roldan, N. H. de Leeuw and C. R. A. Catlow, Carbon dioxide and water co-adsorption on the low-index surfaces of TiC, VC, ZrC and NbC: a DFT study, *Phys. Chem. Chem. Phys.*, 2019, **21**, 10750–10760.

23 Á. Morales-García, M. Mayans-Llorach, F. Viñes and F. Illas, Thickness biased capture of CO2 on carbide MXenes, *Phys. Chem. Chem. Phys.*, 2019, **21**, 23136–23142.

24 M. T. Aswathi, N. Kuriakose, K. Mondal and P. Ghosh, CO2 capture, activation and dissociation on the Ti2C surface and Ti2C MXene: the role of surface structure, *Phys. Chem. Chem. Phys.*, 2020, **22**, 14599–14612.

25 H. Prats, H. Mcaloone, F. Viñes and F. Illas, Ultra-high selectivity biogas upgrading through porous MXenes, *J. Mater. Chem. A*, 2020, **8**, 12296–12300.

26 M. G. Quesne, A. Roldan, N. H. De Leeuw and C. R. A. Catlow, Bulk and surface properties of metal carbides: implications for catalysis, *Phys. Chem. Chem. Phys.*, 2018, **20**, 6905–6916.

27 J. P. Perdew, K. Burke and M. Ernzerhof, Generalized Gradient Approximation Made Simple, *Phys. Rev. Lett.*, 1996, **77**, 3865–3868.

28 G. Kresse and J. Furthmüller, Efficiency of ab initio total energy calculations for metals and semiconductors using a plane-wave basis set, *Comput. Mater. Sci.*, 1996, **6**, 15–50.

29 G. Kresse and J. Furthmüller, Efficient iterative schemes for *ab initio* total-energy calculations using a plane-wave basis set, *Phys. Rev. B: Condens. Matter Mater. Phys.*, 1996, **54**, 11169–11186.

30 G. Kresse and J. Hafner, *Ab initio* molecular dynamics for liquid metals, *Phys. Rev. B: Condens. Matter Mater. Phys.*, 1993, **47**, 558–561.

31 P. E. Blöchl, Projector augmented-wave method, *Phys. Rev. B: Condens. Matter Mater. Phys.*, 1994, **50**, 17953–17979.

32 S. Grimme, J. Antony, S. Ehrlich and H. Krieg, A consistent and accurate ab initio parametrization of density functional dispersion correction (DFT-D) for the 94 elements H-Pu, *J. Chem. Phys.*, 2010, **132**, 154104.

33 S. Grimme, Semiempirical GGA-type density functional constructed with a long-range dispersion correction, *J. Comput. Chem.*, 2006, **27**, 1787–1799.

34 C. Li, J. Kuo, B. Wang, Y. Li and R. Wang, A new layer compound Nb4SiC3 predicted from first-principles theory, *J. Phys. D: Appl. Phys.*, 2009, **42**, 075404.

35 M. Hellenbrandt, The Inorganic Crystal Structure Database (ICSD)—Present and Future, *Crystallogr. Rev.*, 2004, **10**, 17–22.

36 G. W. Watson, E. T. Kelsey, N. H. de Leeuw, D. J. Harris and S. C. Parker, Atomistic simulation of dislocations, surfaces and interfaces in MgO, *J. Chem. Soc., Faraday Trans.*, 1996, **92**, 433.

37 P. E. Blöchl, O. Jepsen and O. K. Andersen, Improved tetrahedron method for Brillouin-zone integrations, *Phys. Rev. B: Condens. Matter Mater. Phys.*, 1994, **49**, 16223–16233.

38 D. M. Többens, N. Stüßer, K. Knorr, H. M. Mayer and G. Lampert, in *Materials Science Forum*, Trans Tech Publications Ltd, 2001, vol. 378–381, pp. 288–293.

39 S. R. Shatynski, The Thermochemistry of Transition Metal Carbides, *Oxid. Met.*, 1979, **13**, 105–118.

40 H. H. Hwu and J. G. Chen, Surface Chemistry of Transition Metal Carbides, *Chem. Rev.*, 2005, **105**, 185–212.

41 H. W. Hugosson, O. Eriksson, U. Jansson, A. V. Ruban, P. Souvatzis and I. A. Abrikosov, Surface energies and work functions of the transition metal carbides, *Surf. Sci.*, 2004, **557**, 243–254.

42 F. Silveri, M. G. Quesne, A. Roldan, N. H. De Leeuw and C. R. A. Catlow, Hydrogen adsorption on transition metal carbides: a DFT study, *Phys. Chem. Chem. Phys.*, 2019, **21**, 5335–5343.

43 Á. Morales-García, A. Fernández-Fernández, F. Viñes and F. Illas, CO2 abatement using two-dimensional MXene carbides, *J. Mater. Chem. A*, 2018, **6**, 3381–3385.

44 M. Naguib, V. N. Mochalin, M. W. Barsoum and Y. Gogotsi, Two-Dimensional Materials: 25th Anniversary Article: MXenes: A New Family of Two-Dimensional Materials (Adv. Mater. 7/2014), *Adv. Mater.*, 2014, **26**, 982.

45 B. Hammer, L. B. Hansen and J. K. Nørskov, Improved Adsorption Energetics within Density-Functional Theory Using Revised Perdew-Burke-Ernzerhof Functionals, *Phys. Rev. B: Condens. Matter Mater. Phys.*, 1999, **59**(11), 7413–7421.

46 J. P. Perdew, A. Ruzsinszky, G. I. Csonka, O. A. Vydrov, G. E. Scuseria, L. A. Constantin, X. Zhou and K. Burke, Restoring the Density-Gradient Expansion for Exchange, in *Solids and Surfaces*, 2007.